Materials Research. 2017; 20(Suppl. 2): 603-620
DOI: http://dx.doi.org/10.1590/1980-5373-MR-2017-0039

Application of Friction Surfacing to the Production of Aluminum Coatings Reinforced with Al_2O_3 Particles

Pedro Henrique Fernandes Oliveira[a], Juan Carlos Galvis[a], Juliana de Paula Martins[b], André Luis Moreira Carvalho[a]*

[a]Departamento de Engenharia de Materiais, Universidade Estadual de Ponta Grossa - UEPG, Ponta Grossa, PR, Brazil
[b]Departamento de Engenharia Química, Universidade Tecnológica Federal do Paraná - UTFPR, Ponta Grossa, PR, Brazil

Received: January 16, 2017; Revised: June 14, 2017; Accepted: October 11, 2017

The aim of this work was to produce deposits of AA6351-T6, reinforced with alumina (Al_2O_3) particles, over a substrate of AA5052-H32 through friction surfacing. AA6351-T6 consumable rods were drilled with one and two holes, which were filled with Al_2O_3 particles posteriorly. To perform the deposition, a conventional KONE KFE-3/BR milling machine was used. The results showed that Al_2O_3 particles increase the hardness values of the produced deposits when compared to those without particle addition. The coatings presented a fine equiaxed grain size distribution, once the grain refinement was nearly 48% lower than the as-received material. Moreover, deposit regions that showed finer grain boundaries also showed a higher volume fraction, which can be related to the particle stimulated phenomenon. Electron backscatter diffraction results showed the occurrence of low angle grain boundary substructures and lattice rotation, indicating that the material undergoes dynamic recrystallization during friction surfacing.

Keywords: *Friction surfacing, Hardness, Dynamic recrystallization, Grain boundary, Particle stimulated nucleation.*

1. Introduction

Friction surfacing (FS) is a solid-state technology based on plastic deformation through which it is possible to joint two different metals or alloys. Its application in the surface engineering field is increasingly growing. During the FS process, a consumable rod with a high rotation speed is pressed against a substrate under an axial load. The heat from the contact between the consumable rod and substrate generates a viscoplastic metal layer at the rod tip, where the material is transferred to the substrate in discrete layers of an elliptical shape. In the FS process, the conditions of pressure and temperature lead to an interdiffusion process resulting in the bonding of the material from the consumable rod to the substrate[1-4]. One of the advantages of FS is the production of coatings with a fine microstructure, which show good wear and corrosion resistance. Once there is no melting of the materials involved, it is possible to joint two dissimilar materials that could not be jointed using other coating technologies that involve melting of one or two of the parts involved[1,2,5,6].

Aluminum alloys have low wear resistance, low surface hardness and high coefficient of friction, which limits the use of these alloys. The alloys of the 5xxx series have magnesium as the main alloying element, which results gain in mechanical strength and makes the alloy hardenable by mechanical work. The 5052-H32 alloy has good weldability and good corrosion resistance in marine atmospheres. The 6xxx series alloys have silicon and magnesium as the major alloying element in quantities necessary for the formation of magnesium silicate (Mg_2Si), making the alloys of this series heat-treatable. One of the main alloys of this group is the 6351, which has good conformability, weldability, machinability and corrosion resistance[7,8].

The mechanical properties of aluminum alloys might become even more attractive with the addition of high hardness particles, which work as reinforcing particles in the metal matrix to produce a metal matrix composite. In this regard, many technologies with approaches in surface engineering are used to produce aluminum matrix coatings with particle reinforcement, such as high energy electron beam irradiation, plasma spraying, chemical vapor deposition, powder sinterization and so on. However, despite conventional technologies, FS has been shown to become a more attractive technique once it is a solid-state process with no melting involved, thereby avoiding any reaction of the materials involved and the formation of second phase particles that impair the composite final properties. Moreover, the intense plastic deformation during FS allows the dispersion and mixture of reinforcing particles inside the metal matrix[2,5,9].

Many researchers have studied the possibility of the production of metal matrix coatings reinforced with high

*e-mail: andrelmc@uepg.br

hardness particles through FS. Gandra et al.[2] produced deposits of AA6082 filled with SiC particles using FS, characterizing the deposits with wear testing, volume fraction analysis of particles inside of the produced deposits and a hardness test of a specific region of the deposits. Karthik et al.[5] studied the production of AA5083 deposits filled with titanium particles, where the deposits showed a fine equiaxed microstructure, good particle dispersion along the deposits and a gain in mechanical resistance due to the insertion of reinforcing particles. Reddy and Mohandas[9] investigated the wear and corrosion resistance of a deposit produced from a metal matrix composite consumable rod A356 reinforced with SiC particles using FS. Shinoda et al.[10] deposited AA5052 consumable rods, filled with Al_2O_3 particles, to obtain a homogeneous distribution of particles in the produced deposit. Nakama et al.[11] showed the increasing of wear resistance of AA6061 deposits reinforced with Al_2O_3 particles produced by FS. There are also studies related to the microstructural transformations that occur during FS. Rafi et al.[6] showed the microstructural evolution occurring in H13 steel, while Vilaça et al.[12] showed the microstructural transformation in a consumable rod during FS. Gandra et al.[13] obtained a refined microstructure with a degree of refinement of 33% after a FS process, Puli[14] related the dynamic recrystallization phenomenon during FS for a austenitic stainless steel and Suhuddin et al.[15] made a brief investigation of dynamic recrystallization of AA6086-T6 during FS.

Nevertheless, further investigations on the influence of reinforcing particles on the properties of the deposits produced by FS, taking into the consideration the relationship with the variation of volume fraction, are required. A more detailed investigation addressing the phenomenon of dynamic recrystallization that occurs during FS processing is also needed[14]. On this basis, the present work aims to carry out a more detailed investigation of the use of reinforcing particles in the deposits produced by FS, showing (i) the dispersion pattern of Al_2O_3 particles in a qualitative and quantitative way, (ii) the relation to the Al_2O_3 volume fraction with the hardness values of the obtained deposits, (iii) a study of the microstructural evolution during the processing through electron backscatter diffraction (EBSD) analysis, with the aim of providing evidence of the occurrence of dynamic recrystallization during FS, and (iv) the Al_2O_3 particle influence on the final microstructure.

2. Experimental Procedure

Plates of AA5052-H32 with 2.5 mm thickness were used as the substrate and consumable rods of extruded AA6351-T6 of 19.05 mm diameter and 130 mm length were used to make deposits. Al_2O_3 particles, with a mean size of 1 μm, were inserted into each rod. Table 1 shows the chemical composition of the aluminum alloys used in the present investigation.

To perform the deposition, a KONE KFE-3/BR conventional milling machine was used, with position control of the three axes of the table machine. Figure 1(a) shows the milling machine used to perform FS. Figure 1(b) indicates the operational set up used to produce the deposits, the table advance direction and upward axial displacement and spindled speed of 4200 rpm capacity.

To fill the rods with Al_2O_3 particles, two arrangements of holes with a 2 mm diameter and a 30 mm depth in each rod were created. The particle filling procedure was performed in a gradual way to ensure that the particles fill the entire length of the hole. Both the holes were made at a distance of 3 mm from the center and in the rods with two holes, the holes were made whilst maintaining a spacing of 180° from each other (Figure 1(c)). The rod hole pattern production was chosen based on the results shown by Gandra et al.[2].

The main control parameter used during FS was the upward axial displacement of the milling machine table, where the substrate was put in constant contact with the consumable rod, allowing the consumption of the rod and production of the deposits. From this, it was possible to calculate the rod feed rate, which can be defined as the velocity that the rod is consumed along the axial direction. The rod feed rate (Vz) is determined from the relationship between the axial upward displacement values of the machine table (Dz) and the total time of deposition (t), given by equation (1):

$$C_R = \frac{\Delta W}{A.t} \qquad (1)$$

The other process parameters used were chosen based on works reported by other authors[1,2,5,9,13,16] and are listed in Table 2.

In Table 2, 1-4 tests correspond to tests performed with one hole and 5-8 tests correspond to those performed with two holes in the consumable rod. For each deposition process (test), two deposits over the substrate were obtained, which totalized sixteen depositions performed.

After production of the deposits, samples were extracted for metallographic analysis, Al_2O_3 volume fraction analysis and measurement of the microhardness profile according to the sample plan extraction shown in Figure 2(a). Three samples of each deposit were extracted from the cross-section with an initial 30 mm, as can be seen in Figure 2(b). Figure 2(c) shows the microhardness profile measurement plan along the substrate, substrate/deposit and deposition interface, in the retreating side, center and advancing side.

The samples for macrostructural analysis were ground with SiC paper (200-600 mesh) and the samples were posteriorly etched with Tucker's reagent. Macrograph images were obtained from an Olympus stereoscope SZ61.

The samples for EBSD analysis were ground with 200-1500 mesh SiC paper. Posteriorly, the samples were submitted to the electrolytic polishing procedure with a polishing machine Buehler ElectroMet 4, using as a polishing

Table 1. Chemical composition of AA5052-H32 and AA6351 alloys used in this investigation.

wt.%	Al	Mg	Si	Cr	Cu	Fe	Mn	Zn
AA5052-H32	97.5	1.87	0.086	0.210	0.009	0.27	0.006	0.003
AA6351-T6	98.1	0.41	0.860	0.003	0.072	0.19	0.420	-

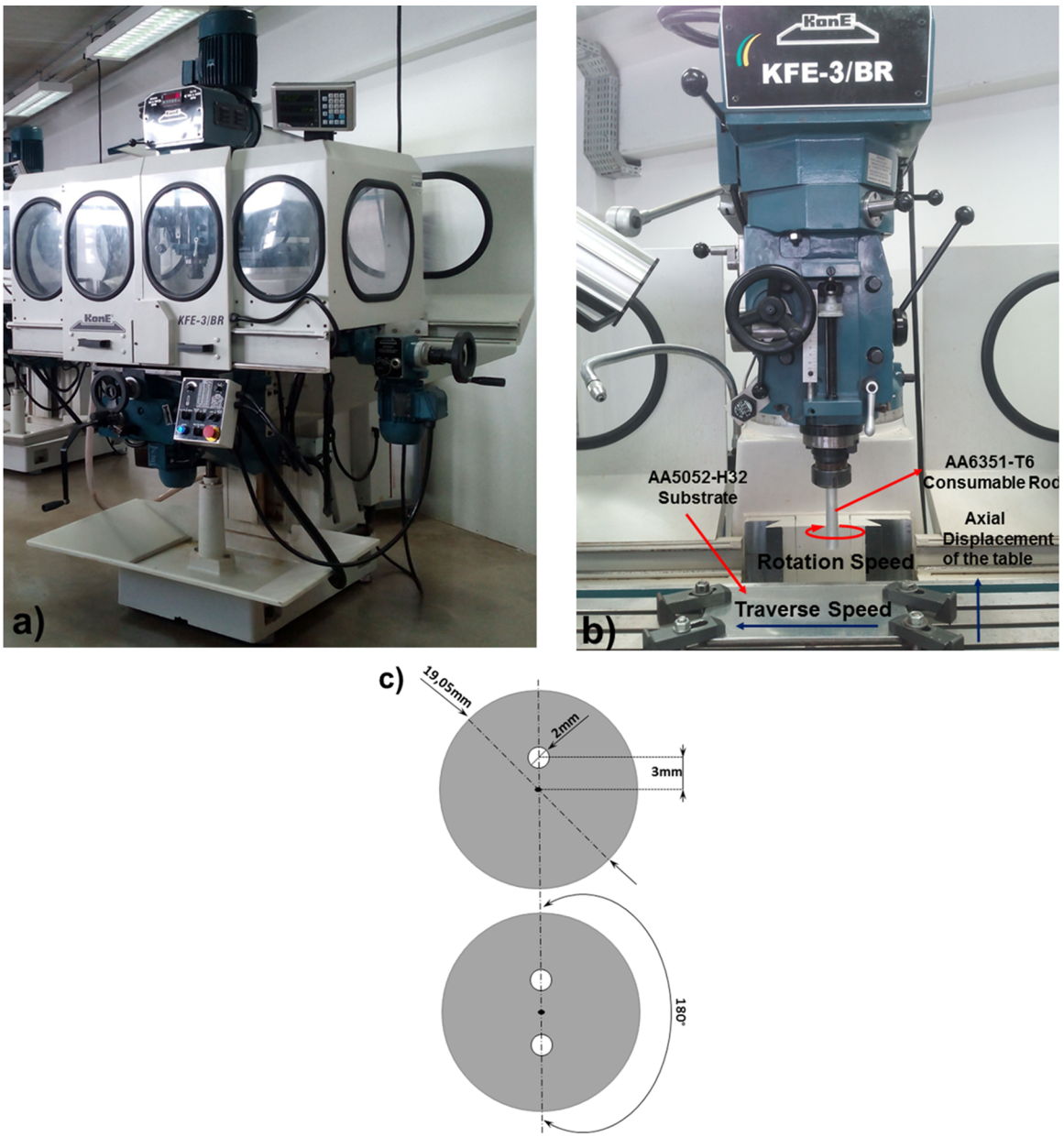

Figure 1. (a) Conventional milling machine used to perform FS, (b) consumable rod arrangement, substrate plate and indications of rotation speed, advancing direction and (c) drilling plan in the consumable rods.

electrolyte, a solution of perchloric acid. EBSD analyzes were performed using a scanning electron microscope with a field emission gun (FEG-SEM) TESCAN Mira 3, using MAMBO and TANGO software for data collection and treatment of the images.

For the microstructural analysis and Al_2O_3 volume fraction determination, the samples were ground and polished in the same steps mentioned above, and after the polishing, the samples were etched by immersion for 30 s in Weck's reagent and then for another 30 s in Keller's reagent. After etching, images were obtained by light microscopy (LM)

Table 2. Rotation speed (rpm) and traverse speed (mm/min) used to perform FS with one (1-4) and two (5-8) holes in the consumable rods.

1 hole in the rod			2 holes in the rod		
Condition	R. Speed (rpm)	T. Speed (mm/min)	Condition	R. Speed (rpm)	T. Speed (mm/min)
1	3000	365	5	3000	365
2	3000	400	6	3000	400
3	3500	365	7	3500	365
4	3500	400	8	3500	400

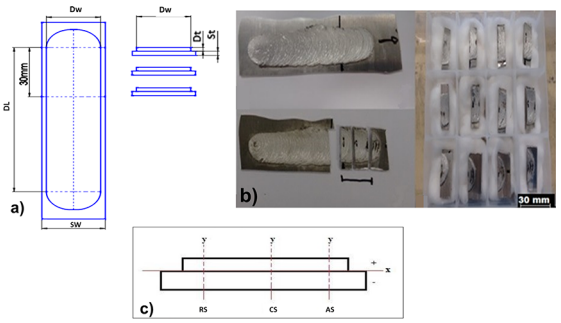

Figure 2. (a) Sample plan illustrating the deposit length (Dt), deposit width (Dw), deposit thickness (Dt) and substrate thickness (Sw). (b) Extracted samples from the initial 30 mm and (c) microhardness profile measurement plan.

Olympus BX51, using bright field mode to obtain the sample microstructure and in the dark field mode for visualization and determination of the Al_2O_3 volume fraction. The Al_2O_3 volume fraction were determined based on ASTM E562-11 standard (Standard Test Method for Determining Volume Fraction by Systematic Manual Point Count).

3. Results and Discussion

3.1 Process control

The main control parameter used to perform FS in the present work was the upward axial displacement of the milling machine table. Hence, from that parameter, the rod feed rate (Vz) was obtained, which was calculated from the relationship between the upward axial displacement of the milling machine table (Dz) and the total time of deposition (t), given by equation (1).

Figure 3 depicts the evolution of the rod feed rate used for the production of the deposits where one might identify four stages during the deposition. In the first stage (time 4 s), the table is put in contact with the rod at high rotation speed, as can be seen in Figure 3(a). In the second stage (Figure 3(b)), due to the continuous upward axial displacement of the table, an initial deformation of the rod with a feed rate of 4.7 mm/s occurs, with this stage occurring approximately in an interval between 4 and 6 s. In this stage, the rod begins to be pressed against the base table, which when associated with the high rotation and heat generation, results in the initial formation of the deposit and flash layer.

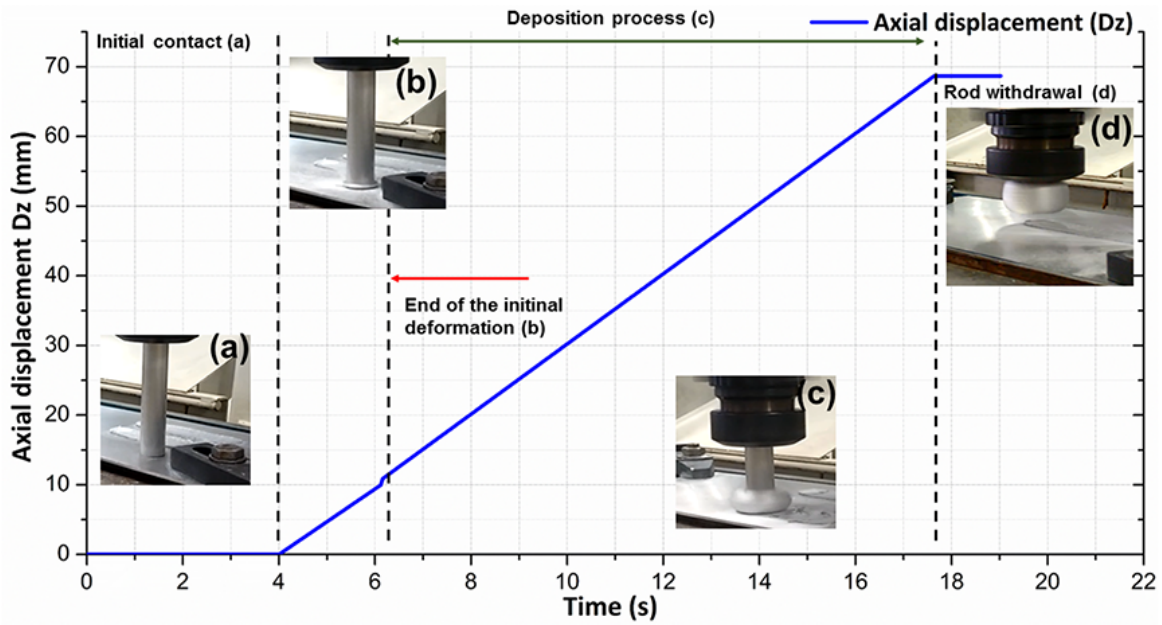

Figure 3. Evolution of rod feed rate with time during FS processing of AA6351-T6 over AA5052-H32. (a) Initial contact, (b) end of initial deformation, (c) deposition process with a constant rod feed rate of 5.03 mm/s and (d) withdrawal from the rod. The deposition was performed with a rotation speed of 3000 rpm and a travel speed of 400 mm/min.

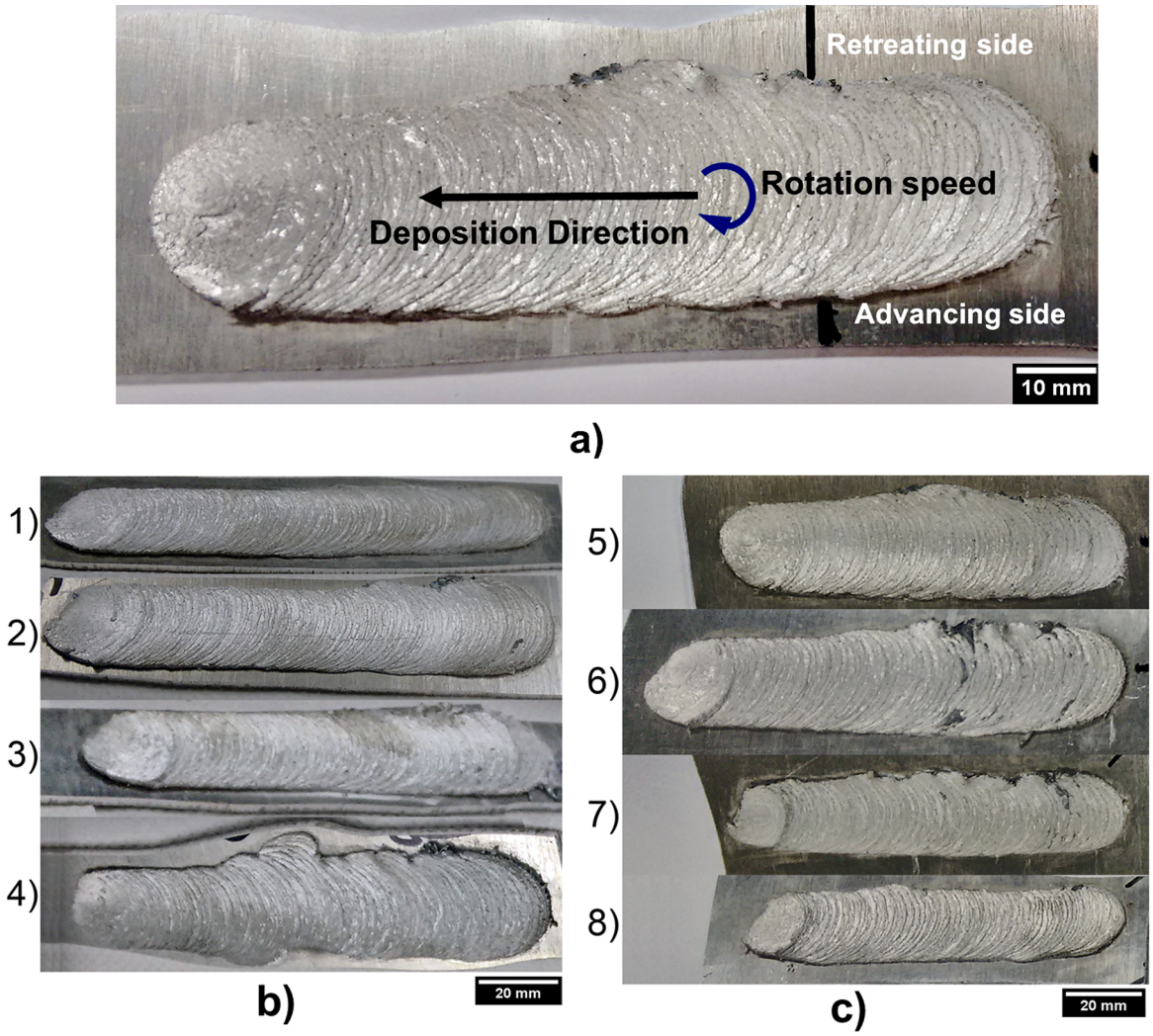

Figure 4. (a) Characteristic processing on the deposit obtained by FS and obtained deposits in the processing conditions with (b) one hole in the rod, conditions 1-4, and (c) two holes in the rod, conditions 5-8.

Table 3. Control parameters and obtained deposit dimensions with one and two holes in the consumable rods.

Control Parameters				Deposit dimensions		
Condition	Dz (mm)	t (s)	Vz (mm/s)	L (mm)	T (mm)	W (mm)
1 (1 hole)	68.595	12.455	5.51	124.80 ± 5.09	2.06 ± 0.23	24.10 ± 0.29
5 (2 holes)	66.715	11.550	5.78	107.57 ± 1.59	2.27 ± 0.18	25.95 ± 0.61
2 (1 hole)	67.085	12.650	5.31	125.90 ± 3.54	1.79 ± 0.28	23.71 ± 0.44
6 (2 holes)	66.520	11.625	5.72	115.70 ± 3.17	2.20 ± 0.37	25.72 ± 0.22
3 (1 hole)	66.930	12.560	5.33	116.20 ± 1.41	1.19 ± 0.05	23.81 ± 0.78
7 (2 holes)	63.695	12.275	5.20	109.00 ± 8.17	1.79 ± 0.09	25.26 ± 0.72
4 (1 hole)	67.835	12.255	5.54	120.75 ± 3.04	1,70 ± 0.07	24.66 ± 2.91
8 (2 holes)	61.370	11.570	5.30	107.23 ± 2.45	1.92 ± 0.04	23.83 ± 1.30

After the end of the second stage, with a processing time of 6.2 s, when the rod is in its viscoplastic state, the movement (400 mm/min) of the equipment table begins and this is characterized as the beginning of the deposition. This represents the third stage with the formation of the deposit layer (Figure 3(c)), where the table moves at a constant speed with a rod feed rate of 5.03 mm/s. It can be noted that in this stage, the calculated rod feed rate, represented by the

blue straight line in Figure 3, remained at the same angular coefficient throughout the deposition. This indicates that the deposition process was performed at a constant rod feed rate.

In the fourth stage (Figure 3(d)), the end of the process occurs when the rod is withdrawn from contact with the substrate after consuming 68.67 mm of the rod in a total deposition time of 17.6 s. Similar results were found in other investigations[1,17].

3.2 Superficial characterization of deposits

Figure 4 depicts one of the deposits produced by FS and also indicates the deposition direction and clockwise movement of the consumable rod. Figure 4(b) shows the obtained deposits in each of the eight processing conditions shown in Table 2. For all deposits, it is possible to observe wave marks on the surface, which is an inherent characteristic of the FS process 1. Surface roughness and the formation of the wave marks are related with the nature of material transfer. The plasticized metal is transferred in discrete layers in an elliptical form and each layer gets deposited one after other. Such a characteristic is also found in the results shown by Gandra et al.[16] and Rafi et al.[4], indicating that the union process on the substrate occurs from the retreating side to the advancing side.

Table 3 shows the control parameters used in FS and also the average lengths (L), widths (W) and thicknesses (T) of the deposits for each condition. Data for deposition time (t) and upward axial displacement of the table machine (Dz) were also obtained in order to determine the rod feed rate (Vz).

According to the data from Table 3, it is possible to observe that the deposition time and length of the deposits decrease for FS with two holes rather than one hole in the consumable rod. For example, condition 1 has a shorter time and lower length of 12.46 s and 124.80 mm than for condition 5 with 11.55 s and 107.58 mm, respectively. Alternatively, this variation is followed by an increase in the thickness of the deposits for the two hole in the rod. For example, conditions 3 and 7 have thicknesses of 1.20 and 1.79 mm, respectively. This indicates a lower stiffness of the rod with two holes that resulted in lower resistance during the deposition process, generating thicker deposits, which in turn resulted in a decrease in the length and time to make the deposits.

3.3 Macrograph analysis of deposits

Figures 5 and 6 depict the macrographs of the samples removed from the initial 30 mm of each produced deposit (Figure 2), showing the bonded width of the samples. The bonded width is the region of the deposit that remains adhered to the substrate 1. The notation used for each sample represents the removed sample from each condition. For example, sample 3.1 represents the first sample extracted from condition 3.

From the macrograph analysis of Figure 5, it is possible to observe that there is a difference in the deposit thickness

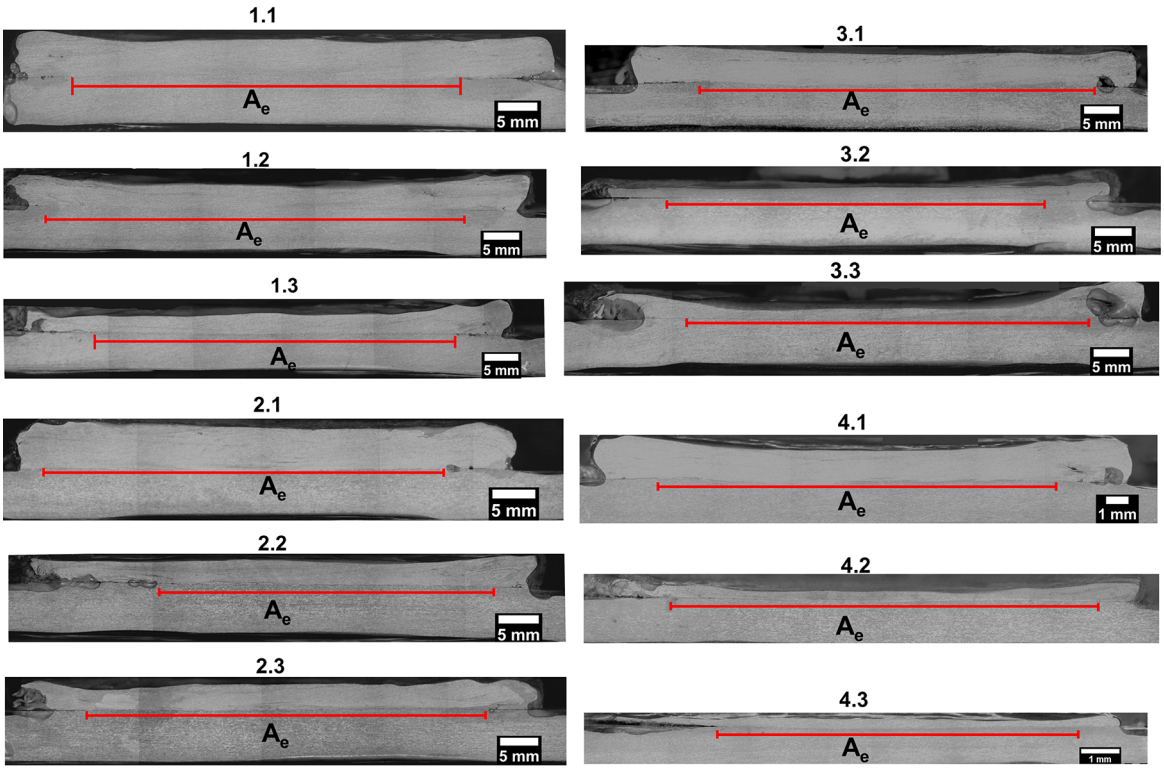

Figure 5. Macrograph of extracted samples from the deposit with one hole in the consumable rod.

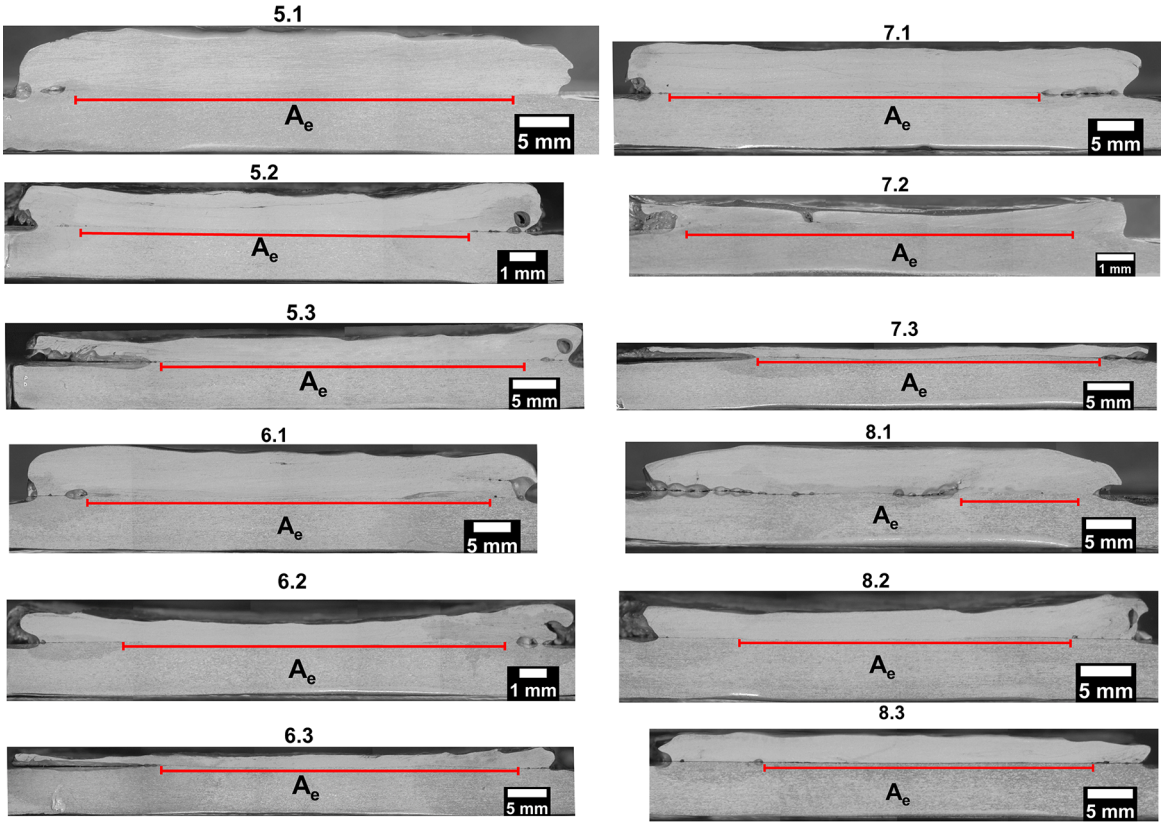

Figure 6. Macrograph of extracted samples from the deposit with two holes in the consumable rod.

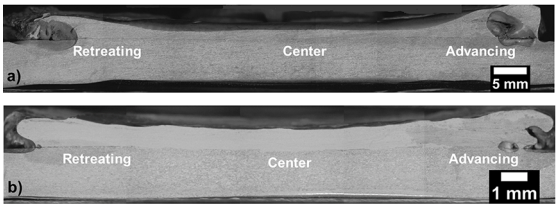

Figure 7. Macrograph showing the difference between the thickness at the center and at the edge of the deposit after FS in conditions (a) 3 and (b) 6.

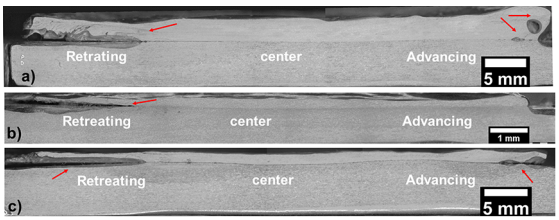

Figure 8. Macrograph showing defects in the retreating side of the deposits of samples (a) 5.2, (b) 4.3 and (c) 7.3.

among samples of the same condition. For example, for samples 4.1, 4.2 and 4.3, the latter has the smallest thickness.

Figure 6 shows the difference in the bonded width among the deposits from the same condition. Consequently, these results indicate that the produced deposits during the processing were not homogeneous.

Furthermore, it is also possible to note that in some conditions, along the deposition, a smaller thickness in the central region with respect to the edge of the deposits occurs, as can be seen in Figure 7 for samples from conditions 3 and 6 (Figure 7(a)) and 7 (Figure 7(b)). This characteristic is likely to be related to the higher resultant axial force as a consequence of the rod feed rate.

Moreover, a predominance of defects in the retreating side of the deposits was observed, as can be seen in Figure 8 (indicated by red arrows). The joint of the deposit to the substrate occurs from the retreating side to the advancing side, hence the majority of defects on the retreating side can be related to the flow material heterogeneously being deposited, once this region is where the adherence process on the substrate begins. This result is similar to that presented by Gandra et al.[16].

Another feature observed was the undercut region in both edges of the deposits. This region represents the part of the deposit that does not adhere on the substrate, although considered as a defect, it is an intrinsic characteristic of the FS. The presence of this defect is due to the viscoplastic metal at the rod tip when it is being pressed against the substrate without lateral restriction. Accordingly, the flow metal at the regions beyond the diameter of the consumable rod create a region with poor adhesion on the substrate[1]. Figure 9 shows

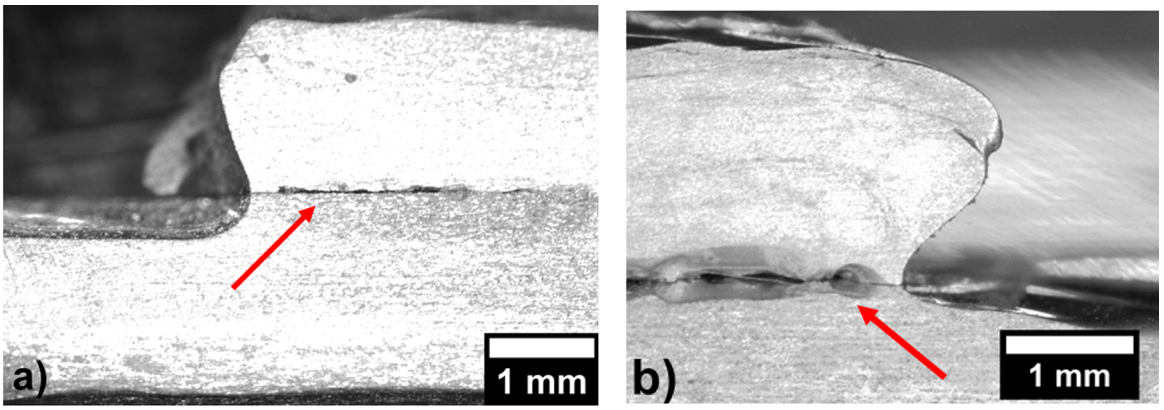

Figure 9. Macrograph showing the undercut region at the edges of deposits in the (a) retreating and (b) advancing sides.

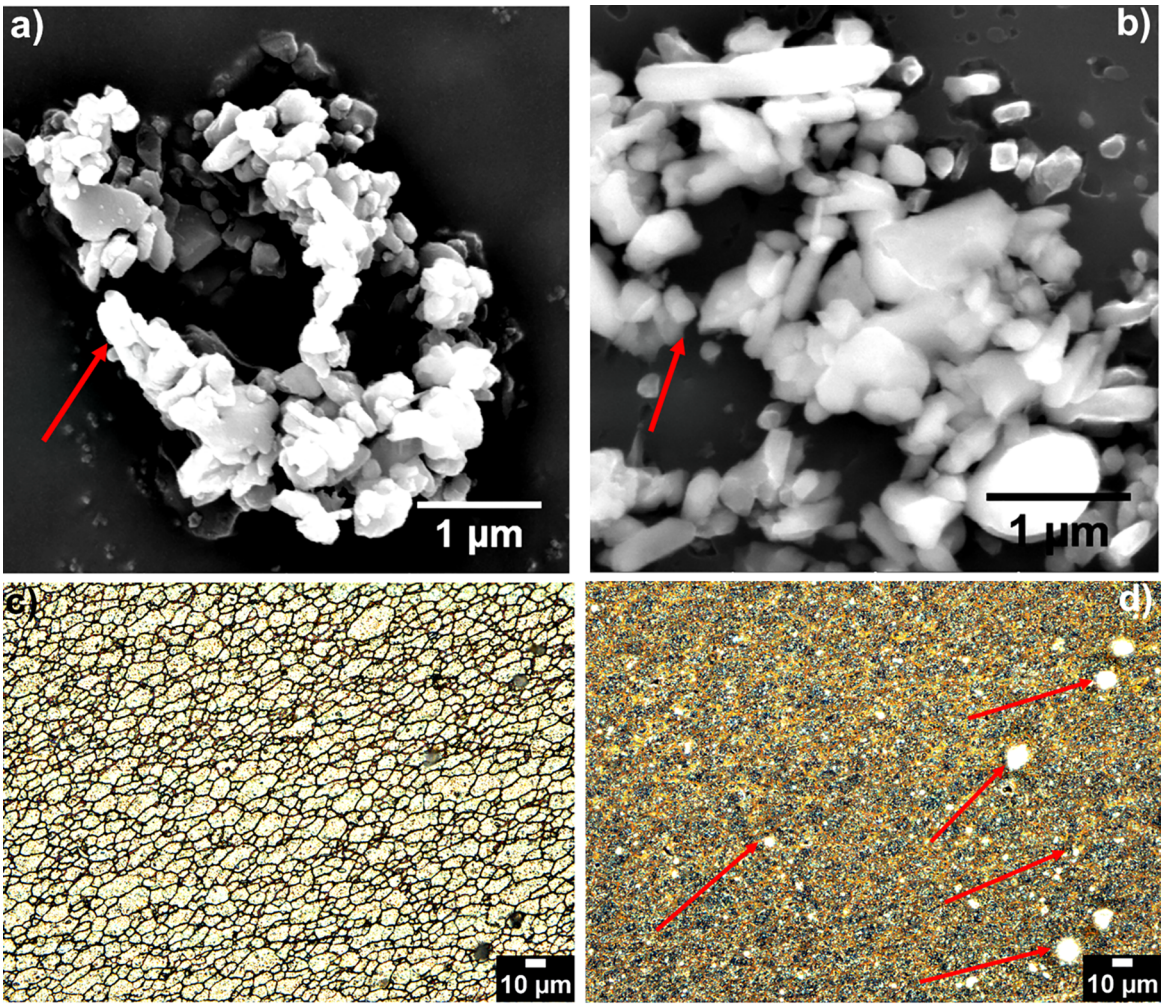

Figure 10. SEM images showing (a) powder Al_2O_3 particles used in FS processing and (b) Al_2O_3 particles inserted into aluminum matrix after FS processing. LM images in (c) bright field and (d) dark field highlighting the Al_2O_3 particles.

the presence of these defects (indicated by red arrows) in the produced deposits.

Furthermore, it was observed that the deposits with two holes in the consumable rod showed more defects and more extensive undercut regions that deposits produced with one hole in the consumable rod, indicating that FS using two holes in the consumable rod needs higher axial loads or rod feed rates than those used in the present investigation.

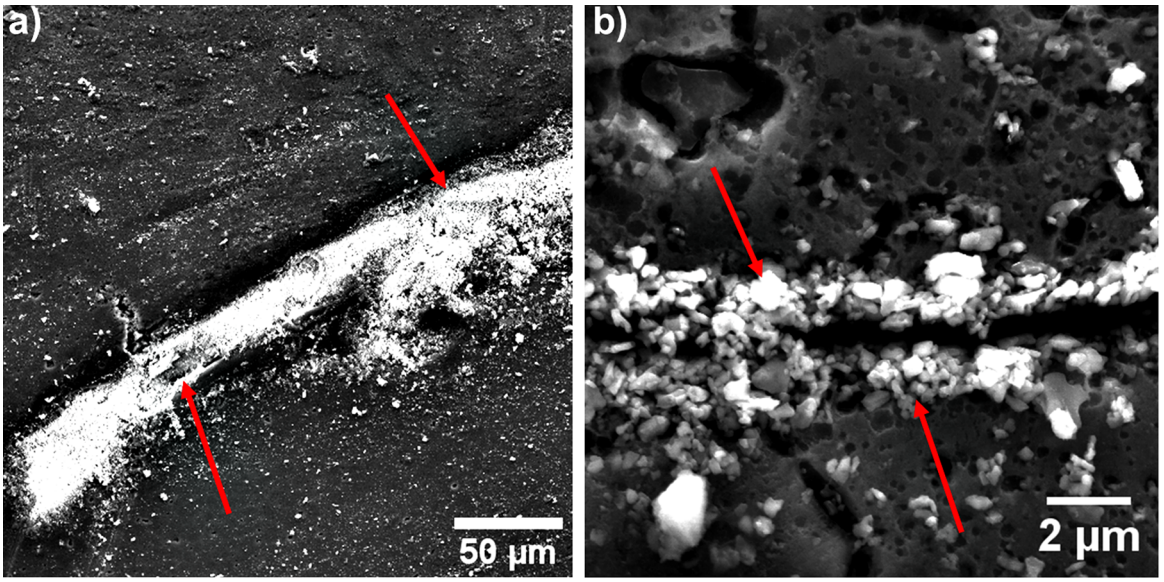

Figure 11. SEM images showing the deposited Al_2O_3 particles in the defects generated in the deposit during FS.

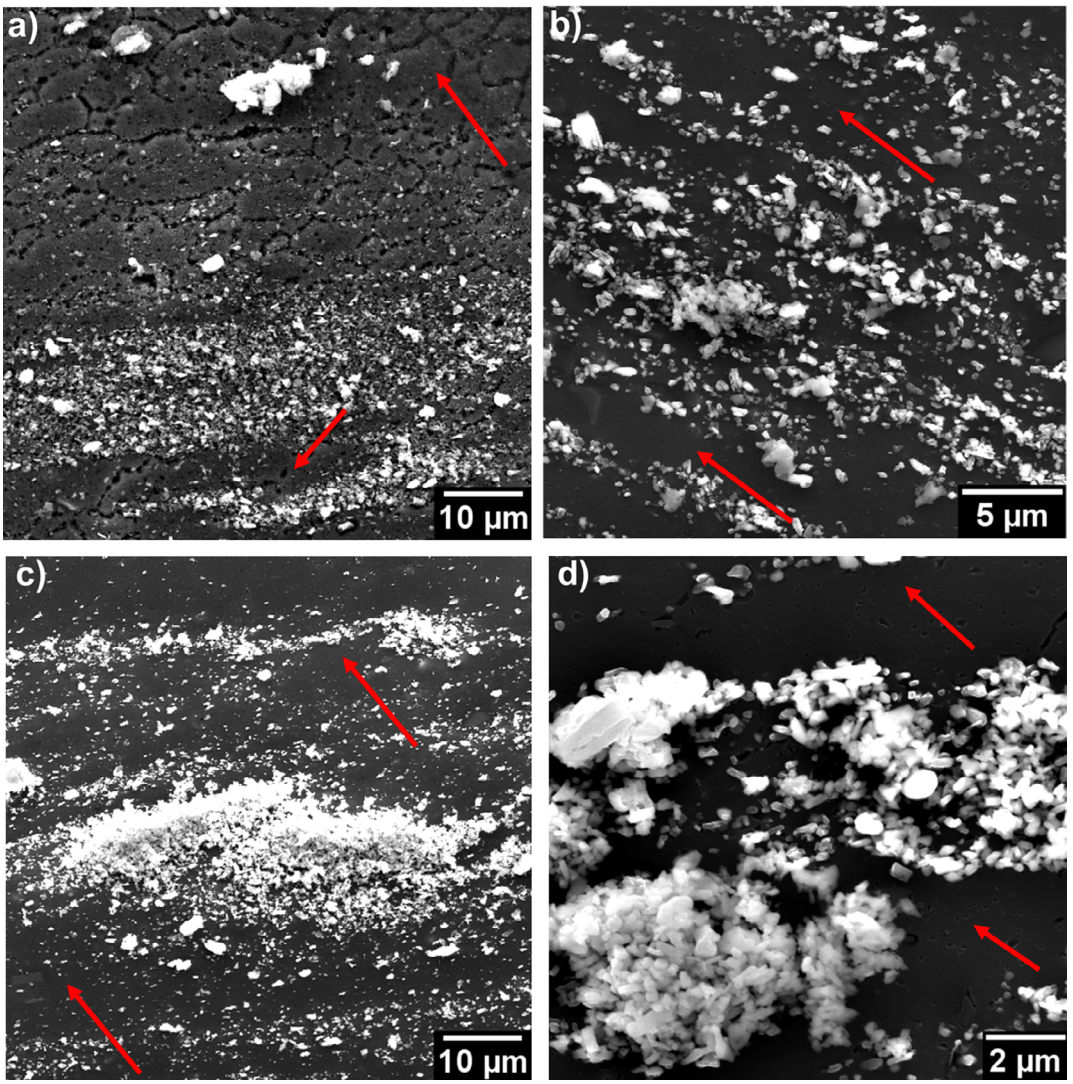

Figure 12. SEM images showing the heterogeneous distribution of Al_2O_3 particles inside the AA6351-T6 matrix.

3.4 Al_2O_3 particles in aluminum matrix

The consumable rods of AA6351-T6 filled with Al_2O_3 particles were used to perform FS to produce deposits of aluminum reinforced with Al_2O_3 particles.

Figures 10(a) and (b) were obtained by SEM and show the powder Al_2O_3 particles (Figure 10(a)) and Al_2O_3 particles inserted in the aluminum matrix after FS processing (Figure 10(b)). It can be noted that the morphology of the particles is identical in both images, indicating that it was possible to insert Al_2O_3 particles into an aluminum matrix through the FS process.

Figures 10 (c) and (d) also depict LM images of the same region, but one in the bright field (Figure 10(c)) and the other in the dark field (Figure 10(d)), indicating (red arrows) that the Al_2O_3 particles can be seen in the microstructure using in dark field mode. The Al_2O_3 particles showed a tendency to be deposited in defects generated along the deposit during the FS, as noted in Figure 11.

The concentration of the particles in the defects is related to the hole in the consumable rod. This concentration occurs because the metal is transferred in discrete layers, hence, the defects can be a consequence of the absence of aluminum in a particular region during the deposition process where instead of the deposition of a metal layer, there is the predominance of the deposition of Al_2O_3 particles. Similar results were found by Gandra et al.[1,2], Sakihama et al.[18] and Chandrasekaran et al.[19].

Another feature that can be noted in the produced deposit is that there was no homogeneous distribution of the particles, that is, the Al_2O_3 particles were concentrated in some regions of the deposit. Figures 12(a) and (d) depict regions with high particle concentrations and regions with an absence of particles (indicated by red arrows), showing qualitative data of the heterogeneous distribution of the particles along the produced deposits.

Table 4. Al_2O_3 volume fraction of deposition performed with one and two holes in the consumable rods.

Condition	% vol.	95% CI	Condition	% vol.	95% CI
1	1.498	0.216	**5**	1.70	0.26
2	1.931	0.366	**6**	1.30	0.16
3	1.821	0.276	**7**	2.37	0.34
4	1.236	0.196	**8**	1.67	0.23

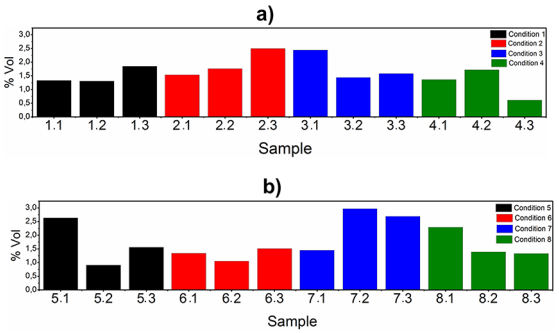

Figure 13. Al_2O_3 volume fraction in each sample from the produced deposits with (a) one and (b) two holes in the consumable rod.

3.5 Al_2O_3 volume fraction

After image processing, it was possible to obtain the volume fraction of Al_2O_3 particles in the deposit after FS. Table 4 shows the Al_2O_3 volume fraction and the 95% confidence interval obtained for the produced deposits with one and two holes in the consumable rod.

As shown in Table 4, among the depositions performed with one hole in the consumable rod, the highest volume fraction of particles inside the aluminum matrix was for condition 2, with a rotation speed of 3000 rpm and a travel speed of 400 mm/min. Whereas, among the depositions performed with two holes in the consumable rod, the highest fraction of particles inside the aluminum matrix was for condition 7, with a rotation speed of 3500 rpm and a travel speed of 365 mm/min. This condition was the highest volume fraction of all depositions investigated.

Also, according to Table 4, with the exception of condition 6, all deposits carried out with two holes in the consumable rod had a higher volume fraction than deposits made with one hole. This is due to the fact that the rods with two roles were filled with a higher amount of Al_2O_3 particles, as expected.

Figure 13 shows the Al_2O_3 volume fraction found in each of the three samples extracted from the produced deposits with one hole (Figure 13(a)) or two holes (Figure 13(b)) in the consumable rod.

It can be seen in Figure 13 that the conditions carried out with one and two holes were found to have different volume fractions in different regions of the deposits. This indicates that the Al_2O_3 particles were deposited in a heterogeneous way along each produced deposit. This agrees with the images in Figure 12, which show regions with high and low concentrations of Al_2O_3 particles in the deposit. Moreover, the heterogeneous distribution of Al_2O_3 particles can also be better observed through the three regions of each sample, as can be seen in Figure 14, which shows a macrograph from sample 3.1 with different volume fractions in the retreating side, center and advancing side.

Figure 14 shows the heterogeneous distribution of particles among the three distinct regions of the deposit. Moreover, it is also possible to note a high difference in the volume fraction found in the same region, as can be seen in Figure 14(a)-(c) for the retreating side. In this case, the region with the higher volume fraction was the retreating side.

Such behavior can also be observed in Figure 15 that depicts different volume fractions in the retreating side, center and advancing side for sample 7.2.

Figure 15 shows a heterogeneous distribution among the regions of the retreating side, center and advancing side of a sample extracted from a produced deposit with two holes

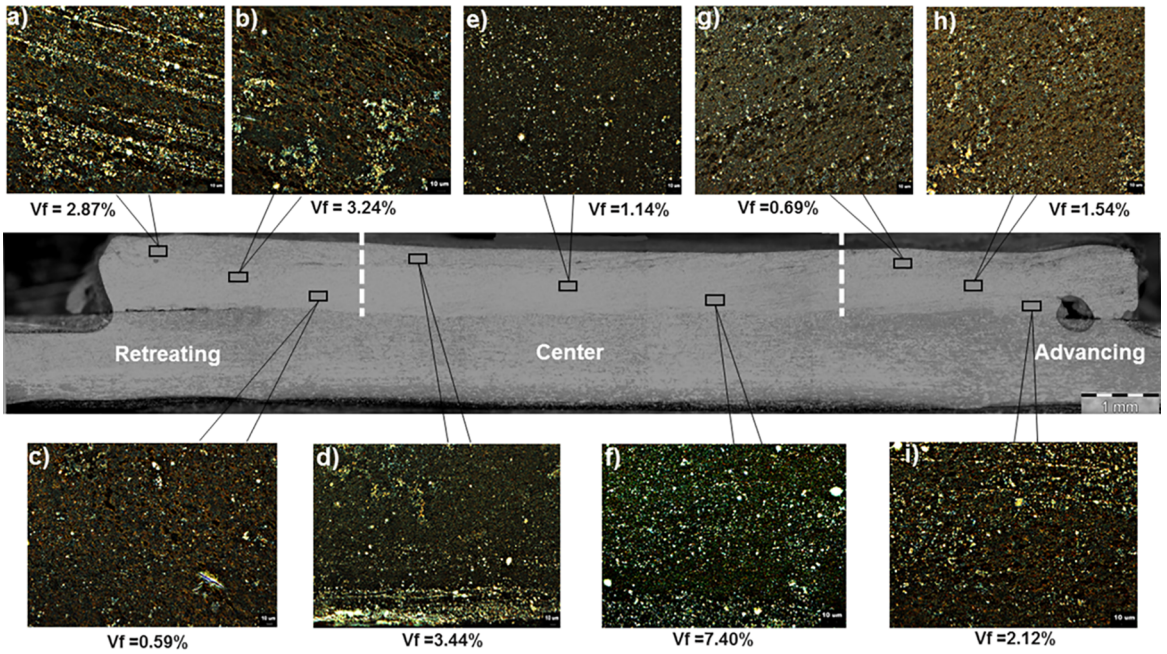

Figure 14. Macrographs of sample 3.1 showing the heterogeneous distribution of Al_2O_3 particles in the (a-c) retreating side, (d-f) center and (g-i) advancing side.

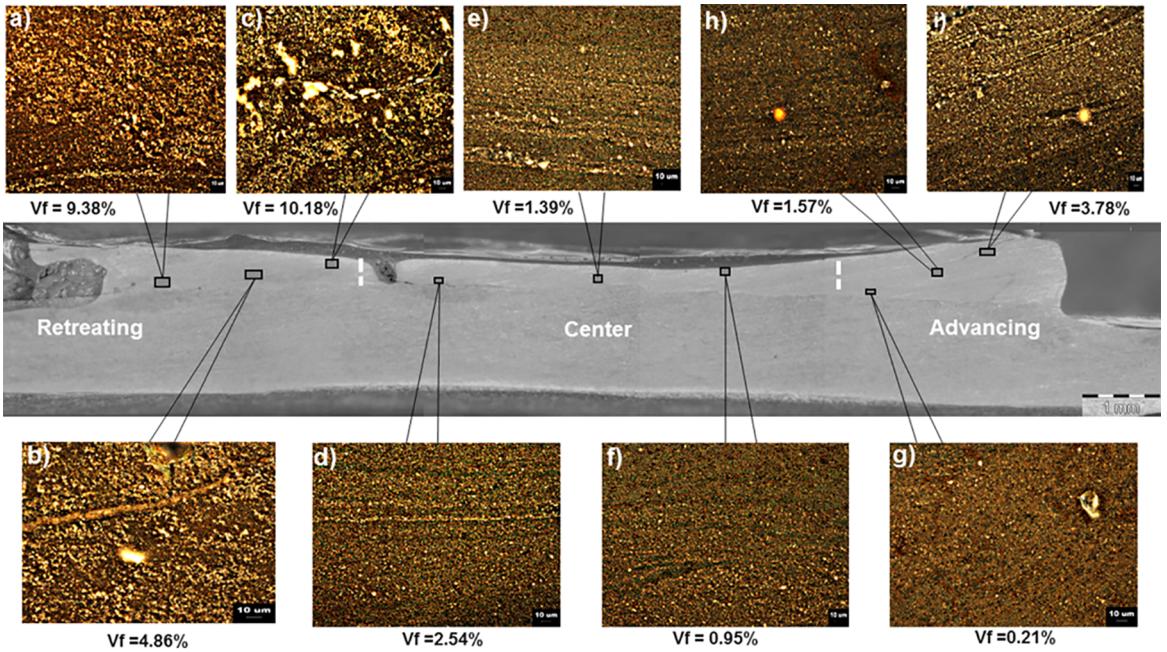

Figure 15. Macrographs of sample 7.2 showing the heterogeneous distribution of Al_2O_3 particles in the (a-c) retreating side, (d-f) center and (g-i) advancing side.

in the rod. Moreover, Figure 15 also shows the difference in the volume fraction values found in the same region, such as the volumetric fractions of the advancing side, as shown by Figures 15 (g)-(i). In this case, the higher volume fraction was found in the center region.

The results shown in Figures 14 and 15 are similar to what was presented in Figures 12 and 13, indicating that there are different volume fractions as a consequence of the heterogeneous distribution of Al_2O_3 particles along the produced deposits with one and two holes in the consumable rods.

Therefore, regarding the volume fraction of Al_2O_3 particles, it was seen that different values of volume fraction are found in different regions of the sample, which contribute to the distribution of particles heterogeneously along the deposit.

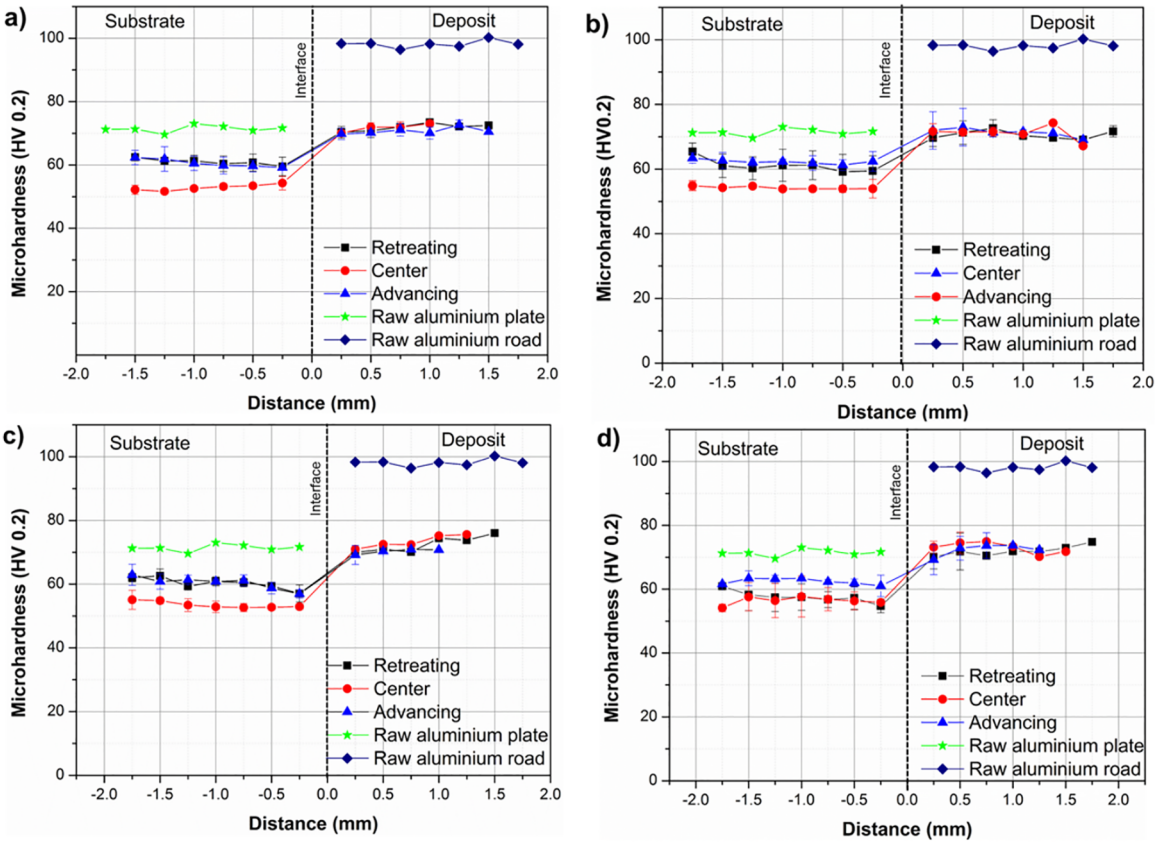

Figure 16. Microhardness profile from conditions (a) 1, (b) 2, (c) 3 and (d) 4.

In this context, more studies are needed to evaluate methods that can contribute to better spreading of the particles in a homogeneous manner along the produced deposit.

3.6 Microhardness profile

The hardness value found for the AA5052-H32 plate substrate is close to 72 HV0.2 and the hardness value for the AA6351-T6 consumable rod is 98.5 HV0.2. The difference in hardness values between the rod and the substrate in the as-received condition was approximately 36%.

The microhardness profiles from each condition were obtained through average hardness values for the retreating side, center and advancing side of each three produced deposit. Figure 16 shows the microhardness profile of each FS condition performed with one hole in the consumable rod.

It can be seen in Figure 16 that the hardness values of the deposit and substrate are lower than the hardness values of the rod and the plate in the as-received condition, respectively. The reason for this change is the loss of the T6 condition of the consumable rod. However, the reduction of the hardness values in the substrate was more pronounced in the central region due to the heat generated during the process, which in turn provides the conditions for recovery and recrystallization phenomena of the deformed grains in the rolling direction, with consequent formation of the heat-affected zone (HAZ).

It was also observed that the produced deposits with one hole in the consumable rod presented hardness values close to 70-75 HV0.2. Thus, it was found that although the volume fraction values were different among the four processing conditions with a hole in the rod, the hardness values found for such deposits were the same. A similar result was reported by Karthik et al.[5].

Alternatively, the hardness values presented for the deposition with one hole in the consumable rod were slightly higher, by approximately 7%, than the hardness values presented for a deposition without the addition of particles. In the work presented by Perez[20] , using the same alloys and without the addition of particles, the hardness values were close to 65-70 HV0.2. This difference can be evidenced due to the particles providing a gain in the hardness of the aluminum matrix.

Figure 17 shows the microhardness profile of each FS condition carried out with two holes in the consumable rod.

From Figure 17, it is possible to observe that the hardness values of the depositions carried out with two holes in the consumable rod were around 75-80 HV0.2. This was approximately 7% higher than the hardness values from one hole in the consumable rod, as shown in Figure 16. In addition, it can be noted that the increase in the hardness of produced deposits with two holes in the rod is followed by an increase in the volume fraction, as shown in Table 4. This

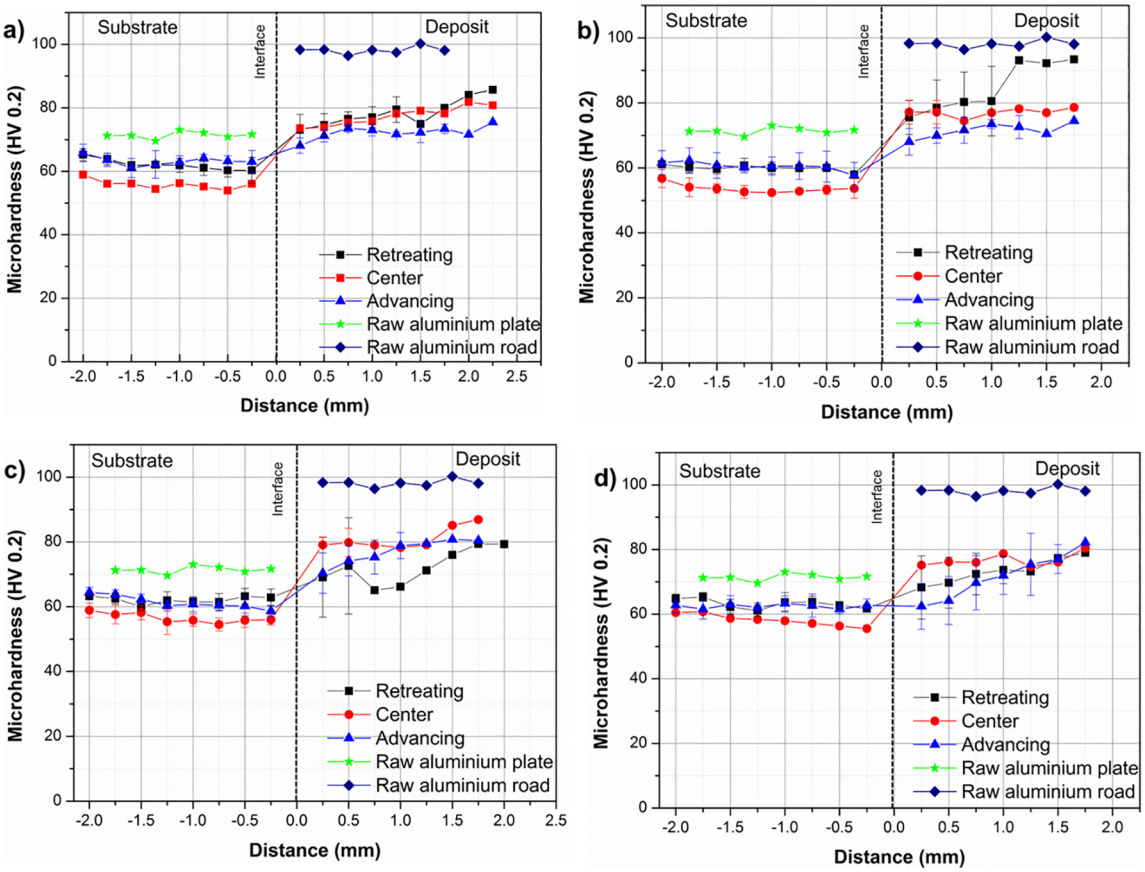

Figure 17. Microhardness profile from conditions (a) 5, (b) 6, (c) 7 and (d) 8.

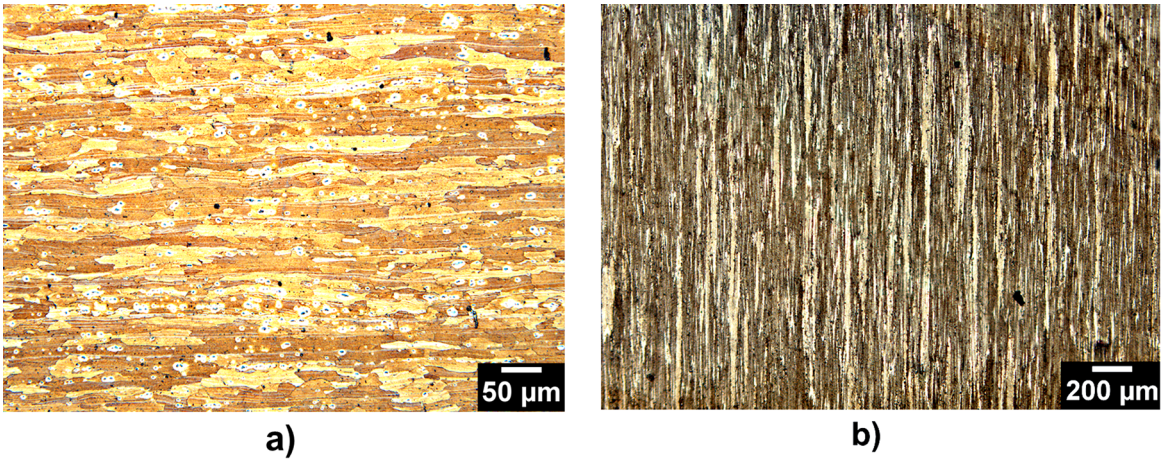

Figure 18. LM images showing the (a) microstructure of the AA5052-H32 substrate and (b) the microstructure of the AA6351-T6 consumable rod in its as-received condition.

indicates that the Al_2O_3 particles contribute to the increase in the hardness of the produced deposits.

On the other hand, for condition 6, the hardness values were not followed by an increase in the Al_2O_3 volume fraction. In this specific case, the volume fraction was lower than for condition 2 and the hardness values were similar. This reveals that there are other factors, such as microstructure and the presence of defects, that can contribute to the variation of the hardness values in each deposit.

Furthermore, the hardness values increase in regions closer to the surface of each deposit. This can be explained by the fact that the heat generated during the FS process dissipates faster in the regions near the surface of the deposits, which possibly affects the microstructural characteristics in this region,

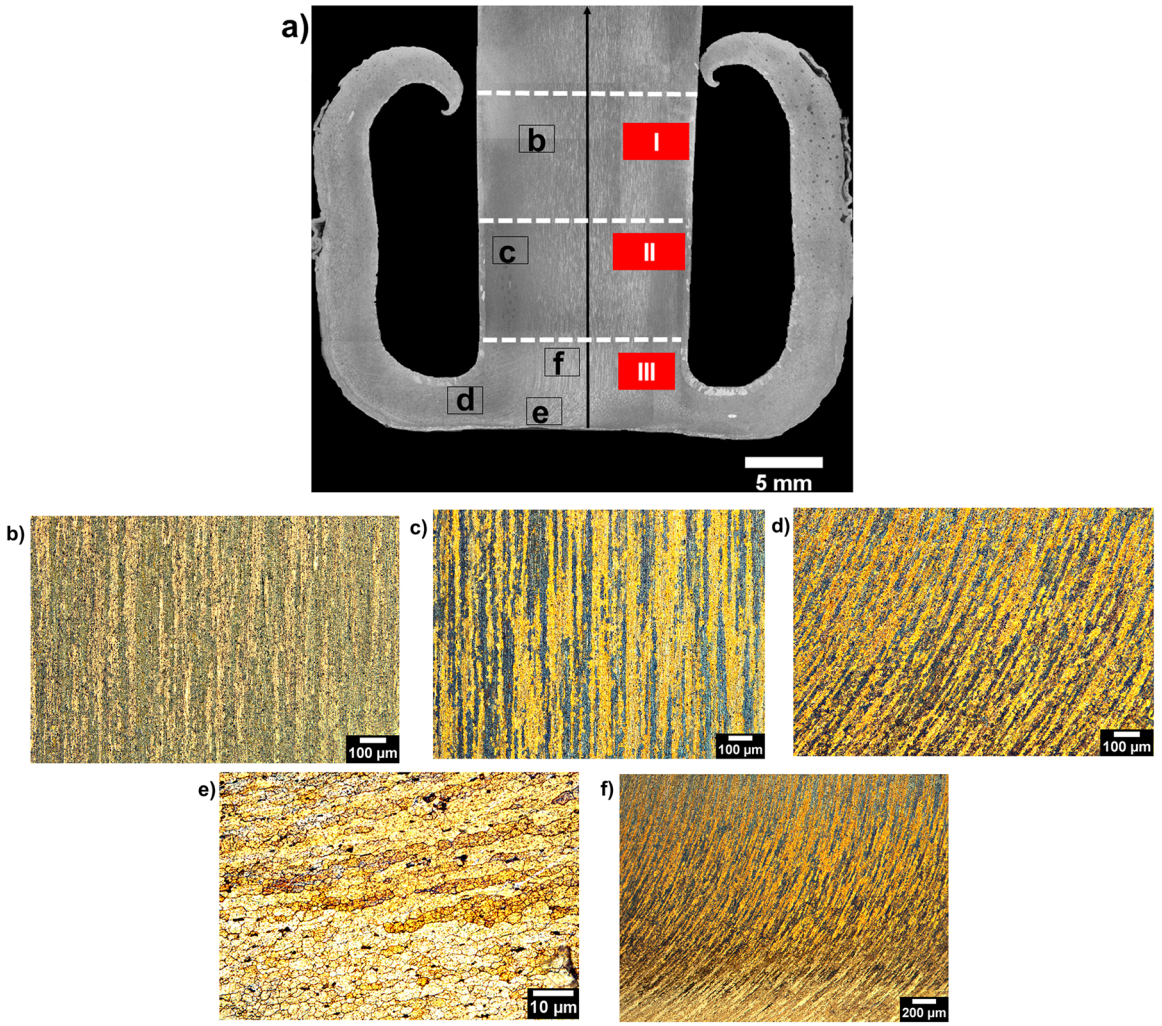

Figure 19. (a) Microstructural evolution of consumable rod. (b) Consumable rod T6 condition microstructure. (c) Microstructure of coarse grains in the HAZ. (d) Grains aligned in the strain direction at the rod tip and (e) and (f) recrystallized grains aligned in the strain direction at the rod tip.

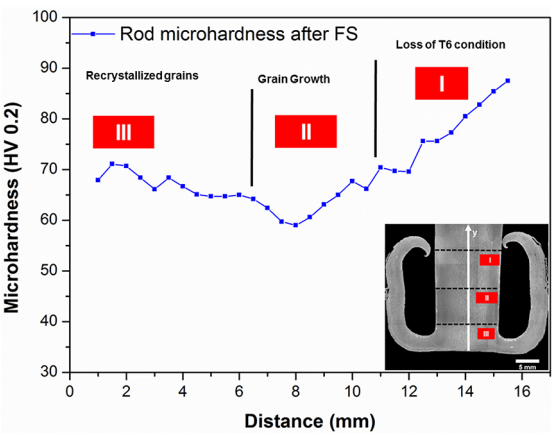

Figure 20. Variation of hardness values along the consumable rod used in the FS process.

inducing a direct effect on the hardness values. The same characteristics were reported by Gandra et al.[6] and Rafi et al.[15].

3.7 Microstructural evolution

Figure 18 shows the micrographs obtained by LM of the AA5052-H32 used as a substrate and the AA6351-T6 used as a consumable rod in its as-received condition.

Figure 18(a) shows the substrate plate microstructure, which reveals strained grains aligned in the rolling direction. It is also possible to note the presence of dark spots, with a shape similar to a "fish eye", which are generated during the electrolytic polishing step where the removal of intermetallic particles from the Al_3Mg_2 or Al_8Mg_5 phases occurred[7]. Figure 18(b) shows the consumable rod microstructure with grains aligned in the extrusion direction.

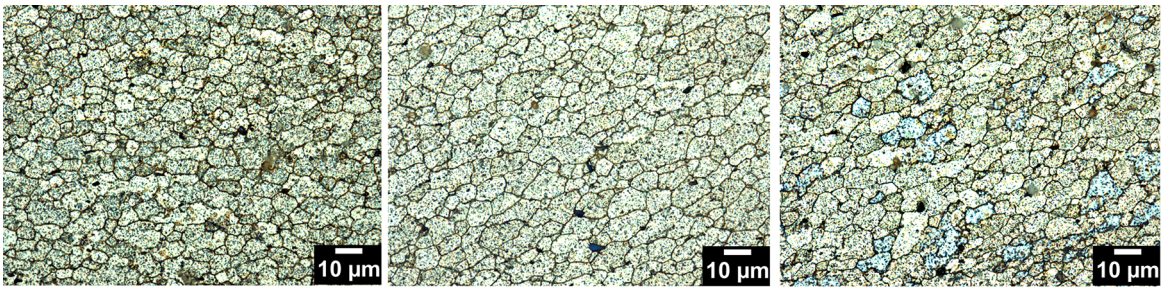

Figure 21. Microstructure of the (a) retreating side, (b) center and (c) retreating side of sample 3.1.

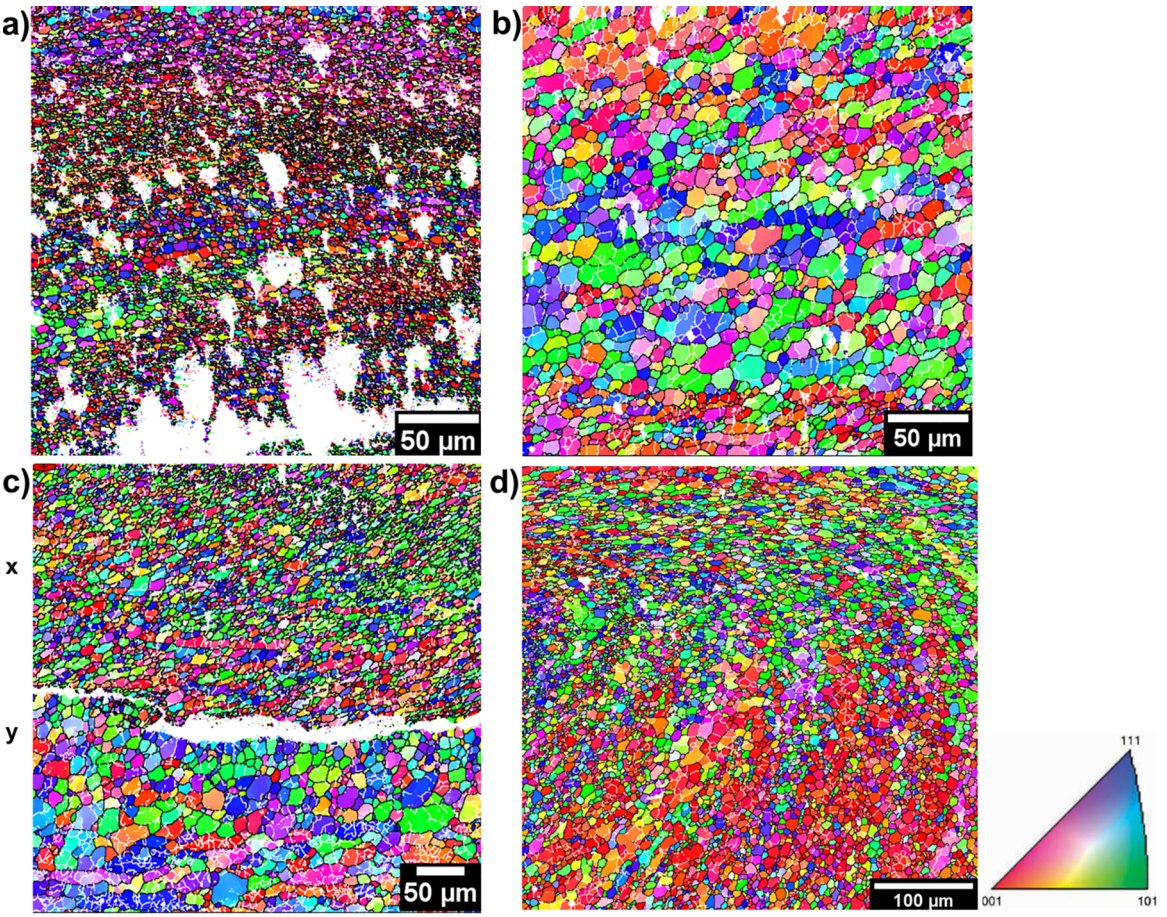

Figure 22. Orientation maps obtained via EBSD of the (a) retreating side, (b) center, (c) center interface deposit(x)/substrate(y) and (d) advancing side of sample 7.2.

Figure 19 shows a longitudinal section from the consumable rod after FS where it is possible to observe the microstructural evolution in the rod during the processing in three different regions. The heat generated by the frictional contact between the rod and substrate is conducted to the upper regions of the rod and creates a temperature gradient along the rod, which determines the degree of deformation along the rod length. Figure 20 depicts the variation of the hardness values along the consumable rod associated to the microstructural changes shown in Figure 19.

According to Figures 19 and 20, it is possible to identify three distinct regions in the consumable rod (Figure 19(a)). In region I, a decrease in the hardness value of the rod (Figure 20) is observed, in relation to the hardness values in the as-received condition, to values around 85-72 HV0.2, which means the loss of the T6 condition. However, in this region, there is no rod microstructural change, once it can be seen that the rod microstructure is similar to the as-received condition (Figure 19(b)).

In region II, the hardness values still decrease, reaching 60-65 HV0.2 (Figure 20), and the microstructure of coarse

Table 5. Results from the average grain size measurements performed in the retreating side, center and advancing side regions for sample 7.2.

Region	Average (μm)	S.deviation	Minimum (μm)	Maximum (μm)
Center	5.66	5.20	0.56	32.19
Advancing Side	4.94	3.65	0.68	67.12
Retreating Side	1.79	1.26	0.62	15.36

Table 6. Results from the average grain size measurements performed in the retreating side, center and advancing side regions for sample 3.1.

Region	Average (μm)	S.deviation	Minimum (μm)	Maximum (μm)
Center	3.79	4.62	0.42	25.00
Advancing Side	4.29	2.73	0.95	34.96
Retreating Side	4.81	3.00	0.98	44.27

grains can be noted (Figure 19(c)). Regions I and II are known as the HAZs of the process, where the drop in the hardness values is due to the loss of the T6 condition and grain growth. These features occur due to the heat generated by the frictional contact between the rod and the substrate.

For region III, it is possible to note a set of deformed grains in the direction of the formation of the flash layer (Figure 19(d)), in addition to a set of recrystallized and equiaxial grains (Figure 19(e)-(f)). In this region, the hot work for the AA6351-T6 consumable rod, where the temperature is associated with compression and torsion forces, provides the conditions for dynamic recrystallization of the material. This phenomenon is followed by a small increase in the hardness values (Figure 20) due to the presence of a refined set of new grains[21]. Gandra et al.[13] found similar results after the FS of a AA2024-T3 alloy.

Moreover, the microstructural evolution that occurred in the deposit was also analyzed. Figure 21 shows the microstructure characteristics of a deposit produced by FS, these images were obtained from the retreating side (Figure 21a), center (Figure 21b) and advancing side (Figure 21(c)) of sample 3.1 (Figure 14).

From Figure 21, it can be seen that the typical microstructure of refined grains is a characteristic of the deposits produced by FS, as consequence of heat and deformation (thermomechanical region), which allow dynamic recrystallization of the material to occur, where the initial set of deformed grains in the extrusion direction of the rod give rise to a set of new equiaxial grains.

In order to obtain more information on the microstructural evolution of the material during FS, EBSD analyzes were performed in some regions of sample 7.2. Figure 22 shows the orientation maps taken from sample 7.2 (Figure 15).

In general, it was possible to observe from the EBSD analyzes (Figure 22), the presence of a refined microstructure of equiaxial grains in the deposit, formed by the fragmentation of the microstructure of the material in its as-received condition due to severe plastic deformation and the frictional heat generated in the FS process. It is also possible to see a change in the morphology of the grains in the substrate. Whereas, the white regions presented in the orientation maps are points not indexed by the analysis of EBSD, which represent the Al_2O_3 particles and low angle grain boundaries (LAGBs), while the high angle grain boundaries (HAGBs) appear in black in Figure 22.

In Figure 22(a), it is possible to observe an excessive concentration of particles in the retreating side which, as previously discussed, is the region that obtained the higher volume fraction of particles for sample 3.1. It was also possible to verify that around some regions with the predominance of Al_2O_3 particles (white regions not indexed in the orientation map), there is a tendency to find grains that are more refined. It is known that micrometric particles, larger than 1 μm in size, can contribute to the occurrence of recrystallization in a phenomenon known as particle stimulated nucleation (PSN)[22]. Due to the high deformation rates involved during the FS process, a high density of dislocations can form around the Al_2O_3 particles, which in turn promote the nuclei of recrystallization around the particles.

Moreover, with the dynamic nature of the recrystallization during FS, generated dislocations can be rearranged to the formation of LAGBs, which have the same mobility and consequently, grow until they become HAGBs. Hence, the higher volume fraction of Al_2O_3 particles in the retreating side shown in Figure 22 can likely contribute to an enhancement in the nuclei of recrystallization, when they become grains with HAGBs and begin to grow over the strained region, but the growth is interrupted when one growth front meets with another[23].

Figures 22(a)-(d) show the HAGBs in black and the LAGBs appear in white. The presence of substructures with LAGBs is evidence of the occurrence of dynamic recrystallization during FS. The LAGBs are associated with the rotation and refinement of cells of dislocations, a decrease of the amount of lattice defects inside and in the walls of cells, followed by classical nucleation mechanisms of recrystallization, such as migration, rotation and coalescing of LAGBs, until the formation of HAGBs[22,24,25].

Furthermore, in Figures 22(b)-(d) it is still possible to observe different tonalities of the same color within some grains, indicating small differences in orientation within

them, which is related to the phenomena of lattice rotation and the formation of substructures. The high density of LAGBs and the small orientation difference within the same grain can probably be related to the fast heat dissipation that occurs during the FS process, which inhibits the formation of HAGBs in some regions.

Figure 22(c) displays the orientation map of the center region of the interface deposit/substrate, the white region between the deposit and substrate reveals a high concentration of Al_2O_3 particles, although it was not possible to index them by the EBSD analysis. Moreover, it is possible to note this in the substrate equiaxial grains near the interface. This feature can be related to the PSN phenomenon and the occurrence of recrystallization. This region of recrystallized equiaxial grains also characterizes the heat HAZ of the substrate and hardness decrease of substrate in regions close to the interface, as seen in the microhardness profiles of Figures 16 and 17.

Alternatively, the presence of LAGBs in the bottom substrate (Figure 22c) is related to the recovery phenomenon, as results a rearrangement of the dislocation cells, preserving the morphology of the deformed grains, which is an expected result for metals with high stacking faults[26].

Table 5 shows the average grain size found in the retreating side (Figure 22(a)), center (Figure 22(b)) and advancing side (Figure 22(d)) of sample 7.2 from Figure 15.

According to the data presented in Table 5, it can be verified that, in spite of the difference of grain size distribution found in specific spots of the deposit, in general, the average grain sizes in the three regions are similar. This shows that FS produces a homogeneous microstructure throughout the deposit, and the small sites that present a difference in grain size can be the result of the presence of Al_2O_3 particles and heterogeneous deformation rates in the region.

However, the retreating side presented a different gran size from those found in other regions of the deposit. This can be related, as previously mentioned, to the 1 μm larger particles that can contribute to the occurrence of recrystallization through the PSN phenomenon, since for sample 7.2, the retreating side had the highest particle concentration.

Thus, the average grain size from the data in Table 6 for the three regions of deposits, referring to the measurements made for sample 3.1 (Figure 14), were similar. It can also be observed in Table 6 that the center region presented a finer grain size than the other regions. This can be related to the larger 1 μm particles that can contribute to the occurrence of recrystallization through the PSN phenomenon, since the central region of sample 3.1 was the one with the highest volume fraction.

Moreover, after the FS process, there was a reduction in average grain size of 48.5%, since the initial grain size of the consumable rod was approximately 9.57 μm.

4. Conclusions

In the present work, we sought to produce AA6351-T6 deposits with the addition of Al_2O_3 particles on a AA5052-H32 substrate through friction surfacing. The deposits were produced using a conventional milling machine, where the main control parameter during deposition was the upward axial displacement of the milling machine table. In addition, the influence of the Al_2O_3 particles on the hardness and final microstructure of the produced deposit was investigated. Based on the presented results it is possible to conclude that:

- It was possible to produce AA6351-T6 deposits with the addition of Al_2O_3 particles over a AA5052-H32 substrate through friction surfacing using a conventional milling machine with the absence of porosity or intermetallics along the retreating, center and advancing regions.
- Friction surfacing with two holes in the consumable rod showed a higher predominance of defects, indicating that for the present case, enhancements in rod feed rates or axial loads are required.
- Friction surfacing with one hole in the consumable rod showed hardness values 21% higher than the hardness found in the substrate and 7% higher than the hardness values compared to the deposition performed without the addition of particles.
- Friction surfacing with two holes in the consumable rod showed an increase in the deposit hardness values of 7% in relation to the deposits with one hole in the consumable rod and this increase of hardness was followed by an increase in the volume fraction of Al_2O_3 particles.
- Friction surfacing produced a microstructure of refined grains and was 48.5% lower when compared to the microstructure of the consumable rod in the as-received condition.
- Friction surfacing with inserted Al_2O_3 particles in the consumable rod contribute to the occurrence of a particle-stimulated recrystallization phenomenon, and accordingly, the enhancement of refined grains in the deposit.

5. Acknowledgments

The authors acknowledge the Coordenação de Aperfeiçoamento de Pessoal de Nível Superior (CAPES) for financial support, the Serviço Nacional de Aprendizagem Industrial (SENAI- Ponta Grossa) for the opportunity and facilities to use the conventional milling machine and UEPG - State University of Ponta Grossa for the opportunity and facilities from the Multiusers Laboratory Complex C-Labmu.

We also thank the Consortium in R&D by Friction Processing (C2PA) of number VDT055-12, which the present research is inserted.

6. References

1. Gandra J, Krohn H, Miranda RM, Vilaça P, Quintino L, dos Santos JF. Friction surfacing-A review. *Journal of Materials Processing Technology*. 2014;214:1062-1093. DOI: http://dx.doi.org/10.1016/j.jmatprotec.2013.12.008

2. Gandra J, Vigarinho P, Pereira D, Miranda RM, Velhinho A, Vilaça P. Wear characterization of functionally graded Al-SiC composite coatings produced by Friction Surfacing. *Materials & Design (1980 - 2015)*. 2013;52:373-383. DOI: http://dx.doi.org/10.1016/j.matdes.2013.05.059

3. Vitanov VI, Javaid N. Investigation of the thermal field in micro friction surfacing. *Surface and Coatings Technology*. 2010;204(16-17):2624-2631. DOI: http://dx.doi.org/10.1016/j.surfcoat.2010.02.003

4. Rafi H, Phanikumar G, Rao KP. Material Flow Visualization during Friction Surfacing. *Metallurgical and Materials Transactions*. 2001;42(4):937-939. DOI: http://dx.doi.org/10.1007/s11661-011-0614-2

5. Karthik GM, Ram GDJ, Kottada RS. Friction deposition of titanium particle reinforced aluminum matrix composites. *Materials Science and Engineering: A*. 2016;653:71-83. DOI: http://dx.doi.org/10.1016/j.msea.2015.12.005

6. Rafi HK, Ram GDJ, Phanikumar G, Rao KP. Microstructural evolution during friction surfacing of tool steel H13. *Materials & Design*. 2011;32(1):82-87. DOI: http://dx.doi.org/10.1016/j.matdes.2010.06.031

7. ASM International. *ASM Handbook Volume 2: Properties and Selection: Nonferrous Alloys and Special Purpose Materials*. Materials Park: ASM International; 2004.

8. Smith WF. *Princípios de Ciência e Engenharia de Materiais*. Lisboa: McGraw-Hill; 1998.

9. Reddy GM, Rao KS, Mohandas T. Friction surfacing: novel technique for metal matrix composite coating on aluminium-silicon alloy. *Surface Engineering*. 2009;25(1):25-30. DOI: http://dx.doi.org/10.1179/174329408X298238

10. Shinoda T, Okamoto S, Takemoto S, Kato Y, Shimizu T. Deposition of hard surfacing layer by friction surfacing. *Welding International*. 1996;10(4):288-294. DOI: http://dx.doi.org/10.1080/09507119609548997

11. Nakama D, Katoh K, Tokisue H. Fabrication of 6061 aluminum alloy/Al_2O_3 particle composites by friction surfacing. *Journal of Japan Institute of Light Metals*. 2008;58(7):299-304.

12. Vilaça P, Gandra J, Vidal C. Linear Friction Based Processing Technologies for Aluminum Alloys: Surfacing, Stir Welding and Stir Channeling. In: Ahmad Z, ed. A*luminium Alloys - New Trends in Fabrication and Applications*. Rijeka: InTech; 2012. DOI: http://dx.doi.org/10.5772/52026

13. Gandra J, Pereira D, Miranda RM, Silva RJC, Vilaça P. Deposition of AA6082-T6 over AA2024-T3 by friction surfacing - Mechanical and wear characterization. *Surface and Coatings Technology*. 2013;223:32-40. DOI: http://dx.doi.org/10.1016/j.surfcoat.2013.02.023

14. Puli R, Janaki Ram GD. Dynamic recrystallization in friction surfaced austenitic stainless steel coatings. *Materials Characterization*. 2012;74:49-54. DOI: http://dx.doi.org/10.1016/j.matchar.2012.09.001

15. Suhuddin U, Mironov S, Krohn H, Beyer M, Dos Santos JF. Microstructural Evolution During Friction Surfacing of Dissimilar Aluminum Alloys. *Metallurgical and Materials Transactions*. 2012;43(13):5224-5231. DOI: http://dx.doi.org/10.1007/s11661-012-1345-8

16. Gandra J, Miranda RM, Vilaça P. Performance analysis of friction surfacing. *Journal of Materials Processing Technology*. 2012;212(8):1676-1686. DOI: http://dx.doi.org/10.1016/j.jmatprotec.2012.03.013

17. Fitseva V, Krohn H, Hanke S, dos Santos JF. Friction surfacing of Ti-6Al-4V: Process characteristics and deposition behaviour at various rotational speeds. *Surface and Coatings Technology*. 2015;278:56-63. DOI: http://dx.doi.org/10.1016/j.surfcoat.2015.07.039

18. Sakihama H, Tokisue H, Kato K. Mechanical Properties of Friction Surfaced 5052 Aluminum Alloy. *Materials Transactions*. 2003;44(12):2688-2694. DOI: http://doi.org/10.2464/jilm.52.346

19. Chandrasekaran M, Batchelor AW, Jana S. Friction surfacing of metal coatings on steel and aluminum substrate. *Journal of Materials Processing Technology*. 1997;72(3):446-452. DOI: http://dx.doi.org/10.1016/S0924-0136(97)00209-4

20. Perez JCG. *Avaliação do processo de deposição superficial por atrito em liga de alumínio AA6351-T6 sobre substrato de liga de alumínio AA5052-H32*. [Dissertation]. Ponta Grossa: Universidade Estadual de Ponta Grossa; 2016. 125 f.

21. Meyers M, Chawla K. *Mechanical Behavior of Materials*. New York: Cambridge University Press; 2009.

22. Humphreys FJ, Hatherly M. *Recrystallization and Related Annealing Phenomena*. 2nd ed. Oxford: Pergamon; 2004.

23. Padilha A, Siciliano F. Crescimento das regiões recristalizadas. In: Tschiptschin A, Padilha Â, Schon C, Langarf F, Goldenstein H, Falleiros I, et al., eds. *Textura e Relações de Orientação*. São Paulo; 2003. p. 71-84.

24. Gonçalves M. Processamento termomecânico e evolução microestrutural de ligas de alumínio: aspectos da metalurgia física fundamental. In: Tschiptschin A, Padilha Â, Schon C, Langarf F, Goldenstein H, Falleiros I, et al., eds. *Textura e Relações de Orientação*. São Paulo; 2003. p. 329-348.

25. De Lima NB, De Lima LMG, Padilha A. Texturas de Recristalização. In: Tschiptschin A, Padilha Â, Schon C, Langarf F, Goldenstein H, Falleiros I, eds. *Textura e Relações de Orientação*. São Paulo; 2003. p. 107-128.

26. Siciliano Júnior F. Recuperação e recristalização durante a deformação a quente. In: Tschiptschin A, Padilha Â, Schon C, Langarf F, Goldenstein H, Falleiros I, et al., eds. *Textura e Relações de Orientação*. São Paulo; 2003. p. 129-150.